Geophysical Research Letters

RESEARCH LETTER
10.1029/2021GL094785

Key Points:

- Advection-driven marine heatwaves (MHWs) are more than three times deeper than surface heatflux driven MHWs on average
- Air-sea heatflux is the dominant driver of MHWs in the East Australian Current jet, whilst advection dominates the extension region
- Advection-driven MHWs are more intense at depth and last four times longer than surface driven MHWs on average

Supporting Information:

Supporting Information may be found in the online version of this article.

Correspondence to:

Y. Elzahaby,
y.elzahaby@unsw.edu.au

Citation:

Elzahaby, Y., Schaeffer, A., Roughan, M., & Delaux, S. (2021). Oceanic circulation drives the deepest and longest marine heatwaves in the East Australian Current system. *Geophysical Research Letters*, *48*, e2021GL094785. https://doi.org/10.1029/2021GL094785

Received 28 JUN 2021
Accepted 13 AUG 2021

Oceanic Circulation Drives the Deepest and Longest Marine Heatwaves in the East Australian Current System

Youstina Elzahaby[1,2], Amandine Schaeffer[1,2], Moninya Roughan[1,2], and Sébastien Delaux[3]

[1]School of Mathematics and Statistics, Coastal and Regional Oceanography Lab, UNSW Sydney, Sydney, NSW, Australia, [2]Centre for Marine Science and Innovation, UNSW Sydney, Sydney, NSW, Australia, [3]MetOcean Solutions, A division of Meteorological Service of New Zealand, Wellington, New Zealand

Abstract Although the impacts of marine heatwaves (MHWs) can extend well below the ocean surface, little is known about how oceanic and atmospheric forcings control their vertical structure. Here, we relate the MHW drivers to their sub-surface characteristics in different dynamical regimes including the East Australia Current. We detect MHWs in the depth-dependent surface mixed layer over 30-years and use a heat budget to identify the dominant mechanisms driving them. We show that MHWs in the Western Boundary Current (WBC) jet are predominantly driven by air-sea heatflux whilst in the WBC extension, MHWs are advection-driven. The deepest and longest MHWs are advection-driven and are more prevalent in autumn and winter. Surface (latent) flux-driven MHWs are shallower and occur predominantly in summer. Demonstrating how MHW characteristics are linked to their drivers facilitates their prediction through driver diagnosis, especially below the surface where observations are sparse and ecological impact is high.

Plain Language Summary Marine heatwaves (MHWs) are extreme ocean warming events that can have devastating ecological impacts on surface and deep ocean communities, yet knowledge of what drives their depth is limited. Here, we identify drivers and characteristics of MHWs on the surface and at depth over the 1985–2014 period in four dynamically different regions of the Tasman Sea. We classify each event's driver and relate it to duration, intensity, seasonality, and depth extent of anomalous warming. We show that MHWs in the Western Boundary Current (WBC) jet are predominantly driven by atmospheric forcing whilst in the WBC extension they are driven by ocean currents through advection. Anomalous advection-driven MHWs are deepest (three times deeper), longest (four times longer) and more prevalent in autumn and winter. This contrasts with atmospherically forced MHWs, which have shallower depth ranges and exhibit a strong seasonal cycle mostly occurring in summer. We also show that the sub-surface intensity extent is not detectable from surface data alone, underscoring the need for sustained sub-surface information. Understanding the dynamical causes and sub-surface structure of the ocean during MHWs is a step toward the prediction of these anomalously warm high impact events.

1. Introduction

Marine heatwaves (MHWs) are extreme ocean warming events that are profoundly detrimental to marine ecosystems and, in turn, local economies. Following the now widely accepted definition proposed by Hobday et al. (2016, 2018), MHWs are discrete, prolonged anomalously warm water events. Numerous studies have covered their impacts, which range from widespread mortality of marine organisms and ecosystem redistribution to severe financial burdens on local fisheries and governments (Salinger et al., 2019; Smale et al., 2019; Wernberg et al., 2013). It has been established that anthropogenic warming is globally linked to MHWs lasting longer, becoming more frequent and more intense (Frölicher et al., 2018; Oliver et al., 2017; Sutton & Bowen, 2019), therefore, understanding their characteristics and drivers is of increasing importance.

MHWs have typically been studied using surface data only (Gupta et al., 2020; Oliver et al., 2019; Wernberg et al., 2013). This is facilitated by the availability of a 30-year (or longer) satellite record of sea surface temperature that allows the identification of daily surface temperature anomalies (Reynolds et al., 2007; Banzon et al., 2016) compared to the scarce record of temperature at depth. However, several studies show

that the events are not restricted to the surface layers and, in fact, the maximum intensities can occur sub-surface. Schaeffer and Roughan (2017) showed that in the coastal Tasman Sea, MHWs could extend to the seabed (~100 m) reaching maximum anomalies around the thermocline. Benthuysen et al. (2018) also found temperature anomalies to be greater at depth (near 60 m) than at the surface during a summer MHW in tropical Australia. Elzahaby and Schaeffer (2019) showed that anomalous warming could extend to depths of 1500 m in the deep ocean. The authors linked the deepest MHWs (>800 m) to anticyclonic eddies in the Tasman Sea and found that they were more prominent in winter. Sub-surface warming has also been shown to linger well after the surface signal has disappeared, indicating that the ocean sub-surface maintains long-term temperature memory (Jackson et al., 2018; Scannell et al., 2020). These findings are consistent with the biological impacts observed from the surface down to benthic communities (Marzinelli et al., 2015; Short et al., 2015).

MHW generation mechanisms vary from atmospheric and local oceanic forcing to large-scale forcing via tele-connections that can modulate temperature extremes. Atmospheric forcing was the primary cause of the 2012 MHW that occurred off the coast of the Northeast US (Chen et al., 2014, 2015), the unprecedented 2013/14 MHW in South America (Rodrigues et al., 2019) and the MHW around tropical Australia in the 2015/16 summer (Benthuysen et al., 2018). These events tended to occur in summer when the water column was highly stratified and the influence of the surface heatflux was mostly restricted to shallow surface layers. In these cases, temperature maximums reached 3°C above monthly climatology and this elevation endured throughout the season. Links between MHW and ocean circulation anomalies have been established for the 2017 MHW in the Middle Atlantic Bight (Gawarkiewicz et al., 2019) and the 2015/16 western Tasman Sea MHW (Oliver et al., 2017). The 2017 MHW lasted for four months and reached a maximum temperature anomaly of 6°C while the 2015/16 extreme warming persisted through 251 days, reaching a 2.9°C anomaly. Atmospheric and oceanic contributions were both found to play roles in generating the 2011 MHW off Western Australia (Benthuysen et al., 2014), which was associated with the 2010/11 La *Niña* (Feng et al., 2013). This event reached a maximum intensity of 6.8°C and lasted for 66 days during the austral summer (Wernberg, 2020).

Heat budgets can be used to identify the dominant mechanisms driving the temperature evolution of the ocean upper layers (Stevenson & Niiler, 1983), and hence to identify the dominant drivers during MHWs. For instance, a heat budget on the continental shelf of Northeast US during the 2012 MHW (using observations and reanalysis) showed inhibited latent and sensible heat loss during the winter, which was attributed to a shift in the atmospheric jet stream leading to anomalously weak wind stress (Chen et al., 2014). Oliver et al. (2017) used a volume-averaged heat budget over a fixed depth of 100 m (also using observations and reanalysis) to show that poleward advection linked to the anomalous East Australian Current (EAC) extension was the dominant contributor to the 2015/16 western Tasman Sea MHW. In the same region, Li et al. (2020) performed a heat budget analysis over the surface mixed layer (also fixed to a depth of 100 m) based on ocean reanalysis data (BRAN2016) from 1994 to 2016. They showed that an increased EAC extension was responsible for 51% of MHWs in the western Tasman Sea.

Western boundary currents (WBCs) are global warming hot-spots (Popova et al., 2016; Wu et al., 2012) where MHWs have been found to be more intense and frequent (Hayashida et al., 2020). WBCs, such as the Kuroshio Current, Agulhas Current and the EAC, are areas of strong poleward advection that are characterised by large sea surface temperature (SST) variability. The Tasman Sea, between the south-east coast of Australia and the west coast of New Zealand, encompasses two contrasting dynamical regimes (Figure 1a). On the west is the EAC, a highly energetic WBC closing the South Pacific subtropical gyre (Hill et al., 2011). The Tasman front, or EAC eastern extension, marks the separation of the EAC from the coast and from the southward meandering EAC southern extension (Oke et al., 2019), which embodies a highly dynamic mesoscale eddy field (Nilsson & Cresswell, 1980; Tranter et al., 1980). In contrast to the EAC system, the eastern Tasman Sea near New Zealand is less dynamic. This part of the Tasman Sea forms the intersection of the Tasman Front, the Subtropical Front and the Subantarctic Front (Behrens et al., 2020; Heath, 1981; Smith et al., 2013).

This study presents a three-dimensional view of MHW characteristics, vertical structure and drivers from 1985 to 2014 using data from a $1/10^{th}$ degree ocean model (Bluelink OFAM3) in the Tasman Sea. We use a daily heat budget over a time-varying mixed layer depth to identify the mechanisms driving temperature

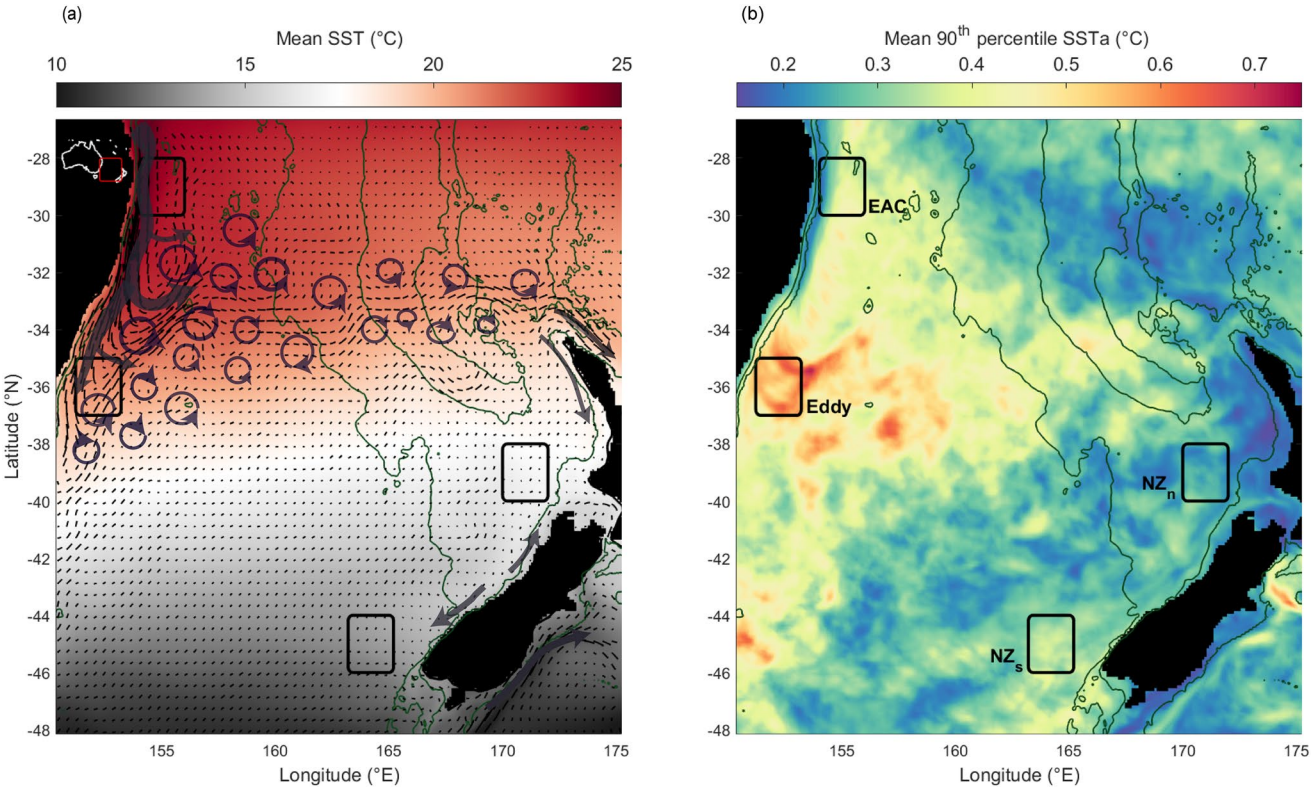

Figure 1. Mean fields (1985–2014) of modeled sea surface temperature (a) and the 90^{th} percentile temperature anomaly (b) in the Tasman Sea. Black vectors show the relative magnitude of currents in the mean state and green lines show 200 and 2000 m bathymetry contours. As marked, the study boxes are: East Australian Current (154°–156°E, 28°–30°S), Eddy (151.2°–153.2°E, 35°–37°S), NZ_{north} (170°–172°E, 38°–40°S) and NZ_{south} (163.2°–165.2°E, 44°–46°S).

variability during MHWs in four dynamically different regions. We characterize the relationship between physical drivers and MHW vertical extent and characteristics both at the surface and throughout the water-column to 1,500 m depth.

2. Materials and Methods

2.1. Data Sets and Study Area

We used the Ocean Forecasting Australian Model version 3 (OFAM3) daily output for the period of 1985–2014, which has been shown to perform well in the Australasian region (e.g., Rykova & Oke, 2015; Feng et al., 2016; Hayashida et al., 2020 amongst others). A comprehensive technical description of OFAM3 is given in Oke et al. (2013). It is a near-global, eddy-rich model with 0.1° horizontal grid resolution and 51 non-uniform vertical layers (5 m in the upper layers and increasing with depth), forced with ERA-Interim (Dee & Uppala, 2009). This model is a configuration of the Geophysical Fluid Dynamics Laboratory (GFDL) Modular Ocean Model (MOM4p1, Griffies et al., 2009).

We chose a non-assimilated model to use in quantifying our heat budget because some assimilation approaches can violate conservation principles and as such introduce uncertainty in the governing physical equations (Stammer et al., 2016). Moreover, Pilo et al. (2019) showed that when quantifying MHWs, eddy rich models, like OFAM3 (0.1°), perform best both regionally and globally. This is particularly pertinent in WBCs (Hayashida et al., 2020) where the mesoscale circulation is essential for driving temperature extremes.

Daily mixed layer depth (MLD) was calculated from the model output using the formulation of de Boyer Montégut (2004) as the depth at which the potential density increases by 0.3 kg m^{-3} and temperature decreases by 0.2°C from the reference depth of 10 m. We found that using a varying MLD resulted in smaller

residual in the heat budget than applying a fixed depth due to the ML encompassing much of the vertical terms in the heat budget.

We identified four sub-regions for our study that represent different dynamical regimes (Figure 1a), namely EAC (in the WBC jet region), Eddy (in the WBC eddy field or southern extension region), NZ_{north} and NZ_{south} both off the west coast of New Zealand. The EAC box encapsulates the fast EAC jet upstream of its bifurcation and exhibits high temperature anomalies. The Eddy box captures the extreme temperature anomalies in the eddy field of the EAC southern extension. Around New Zealand, the southern box captures high SST anomalies of similar intensity to those seen in the EAC box despite the absence of energetic currents in this region (Figure 1b) while the northern box is in a neutral region in terms of anomalies and therefore is chosen for comparison.

Satellite SST from National Oceanic and Atmospheric Administration Optimum Interpolation data set (NOAA OISST V2.1; Reynolds et al., 2007; Banzon et al., 2016, 2020; Huang et al., 2021) covering our study period (January 1, 1984-December 30, 2014) was used for a comparative analysis of OFAM3 surface temperatures over the Tasman Sea region (28°–48°S, 150°–175°E).

Sub-surface temperature profiles from Argo observations (Roemmich et al., 2009) were compared to their equivalent model profiles for each box. We examined 551 profiles in total, 200 in the EAC, 247 in the Eddy region and 104 in NZ_{south} (Figure S2). No profiles were available in the NZ_{north} region, which could be due to the area being shallow.

A MHW was defined as a period when the temperature in the surface mixed layer exceeded the 90^{th} percentile for a consecutive five-day period or longer based on a 30-year baseline climatology (here 1985–2014) as per Hobday et al. (2016). Using OFAM3 model output, the daily varying surface mixed layer temperature was spatially averaged in each box and used as a single temperature time-series to produce the daily climatology and the 90^{th} percentile anomaly. Each MHW was identified over the 30-year period and when individual events were separated by one or two days, they were amalgamated into a continuous event, as per the definition. MHW start/end dates, mean and cumulative intensities and duration were then used to characterize individual events.

To determine the depth structure of each event, the full vertical temperature profile averaged over the box and the duration of each MHW was analyzed. A linear detrend was applied to temperature anomalies at each depth before the analysis of the MHW vertical extent in order to determine the warming extent at depth that is due to the MHW rather than other influences. Otherwise, trends in temperature anomalies were retained in the MHW and heat budget analysis. The MHW depth extent was defined as the depth at which 95% of the profile's heat content anomaly occurred, similar to Elzahaby and Schaeffer (2019)'s identification of anomalous warming depth extent (applied to instantaneous Argo float temperature profiles). Here, the threshold cut-off was slightly altered (previously used 90%) to account for the facts that the temperature data used had already undergone a linear detrending and was averaged in time and space.

2.2. Heat Budget and Anomalies

We calculated a daily heat budget from the model output to use as an instrument for investigating the mechanisms controlling temperature variability in the mixed layer during MHWs. We quantified each of the heat budget terms (as outlined below) daily in each grid cell for the period of 1985–2014. The heat budget represents the heat exchange processes based on the fundamental laws of conservation (Stevenson & Niiler, 1983) and is defined as follows:

$$\frac{dT}{dt} = -\mathbf{u}.\nabla_H T + \frac{Q_{net} - q(h)}{\rho c_p h} + Residual,$$

where $\frac{dT}{dt}$ is the temperature tendency and $\mathbf{u}.\nabla_H T$ is the horizontal advection. Q_{net} is the net air-sea flux (such that positive fluxes are directed into the ocean), and ρ and c_p (1027 kg m^{-3} and 3850 J$(kgC)^{-1}$) are the water density and specific heat capacity, respectively. The heat loss by the shortwave radiation that penetrates below the mixed layer is given by $q(h)$ assuming an exponential decay of surface shortwave radiation with 25 m e-folding depth (Schlundt et al., 2014; Wang & McPhaden, 1999) and h is the daily varying mixed

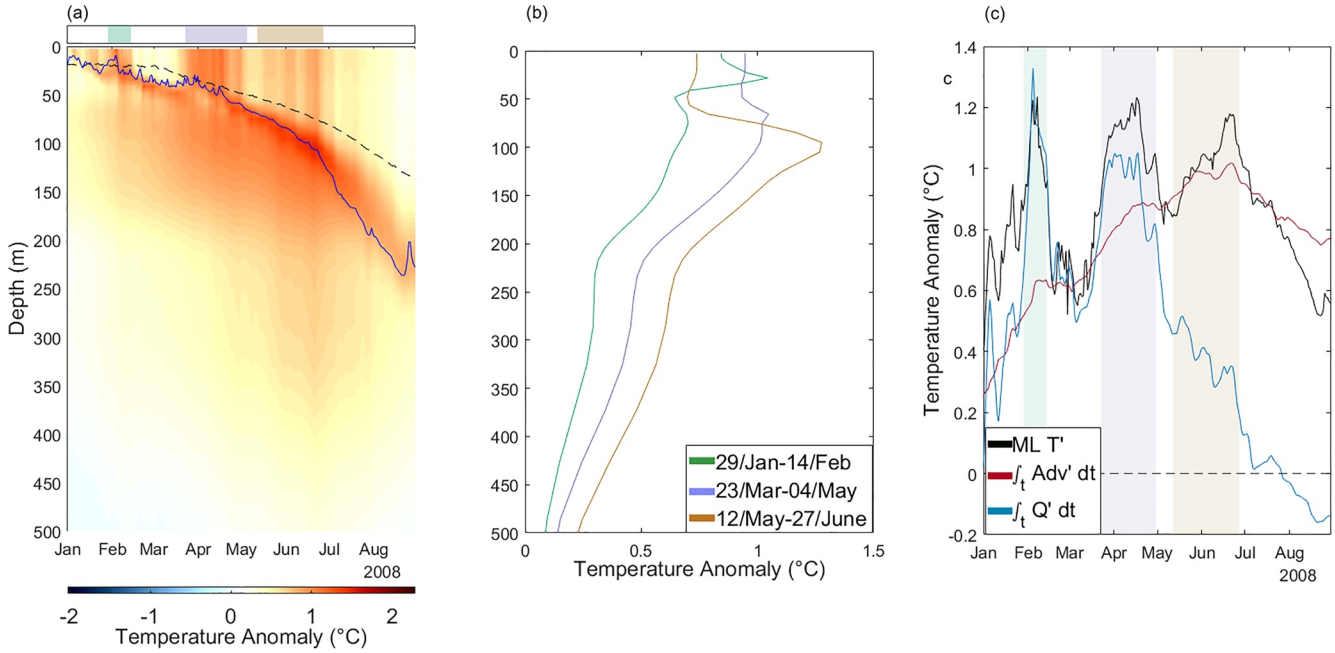

Figure 2. An example from 2008 showing the process of identifying marine heatwaves (MHWs) based on mixed layer depth (MLD) temperature anomaly, vertical profile and classification by driver. (a) Temperature anomalies to 500 m with MHWs marked with rectangles above corresponding to their dominant driver as classified in panel c. Climatological MLD is in black dashed line and daily MLD is shown in solid blue. (b) The vertical temperature anomaly profiles across the top 500 m averaged over the duration of each of the three MHWs identified (color codes corresponding to drivers as identified in panel c). (c) The cumulative air-sea heatflux (blue line), advection (red line) and mixed layer temperature anomaly (black line) are shown with the classification of the MHW as indicated by the highlights (green = Q'-MHW, purple = Mixed MHW, and brown = Adv'-MHW).

layer depth. Residual is the sum of vertical advection and horizontal and vertical diffusion. This term also includes computational uncertainty.

To understand the drivers of MHWs, we focused on heat budget anomaly diagnostics, where the anomalies were calculated based on deviations from daily climatologies of temperature (T'), advection (Adv') and air-sea heatflux (Q'). Climatologies and anomalies were calculated over each grid cell for all terms, which were then volume averaged (over the depth of the daily MLD and per box) and integrated in time (over the event duration) to produce a total anomaly per term for each MHW event.

Finally, the MHW drivers were classified based on the respective contribution of Adv' and Q' to the mixed layer temperature tendency anomaly during each event (Bowen et al., 2017; Chen et al., 2015). They were classified as: advection-driven if the total Adv' was the dominant anomaly during the MHW (hereafter, Adv'-MHW), air-sea heatflux-driven if Q' was the dominant anomaly (hereafter, Q'-MHW) and "mixed" if the difference between the contribution of Adv' and Q' was 10% or less. If neither mechanism was positive during the event, then it was classified as residual-driven and the profile was not included in any further analysis. Figure 2 is a 2008 NZ_{south} excerpt that illustrates the process of MHW identification in the mixed layer (a), vertical propagation (b) and driver classification (c). In this example, three MHWs were detected in 2008, and classified as Q', mixed and Adv'-MHWs. The Adv'-MHW shows the weakest surface signal but is the most intense at depth.

3. Results

3.1. Marine Heatwaves and Heat Budget

Comparative analysis showed consistency between modeled ocean temperature (used to investigate MHWs) and observations. Surface temperature anomalies from OFAM3 and observations from NOAA OI SST (calculated as deviations from their respective 30-year daily climatology, Figure S1) were compared and yielded a highly significant relationship with $r = 0.89$ correlation (p-value $\ll 0.05$) and 0.19°C root mean square

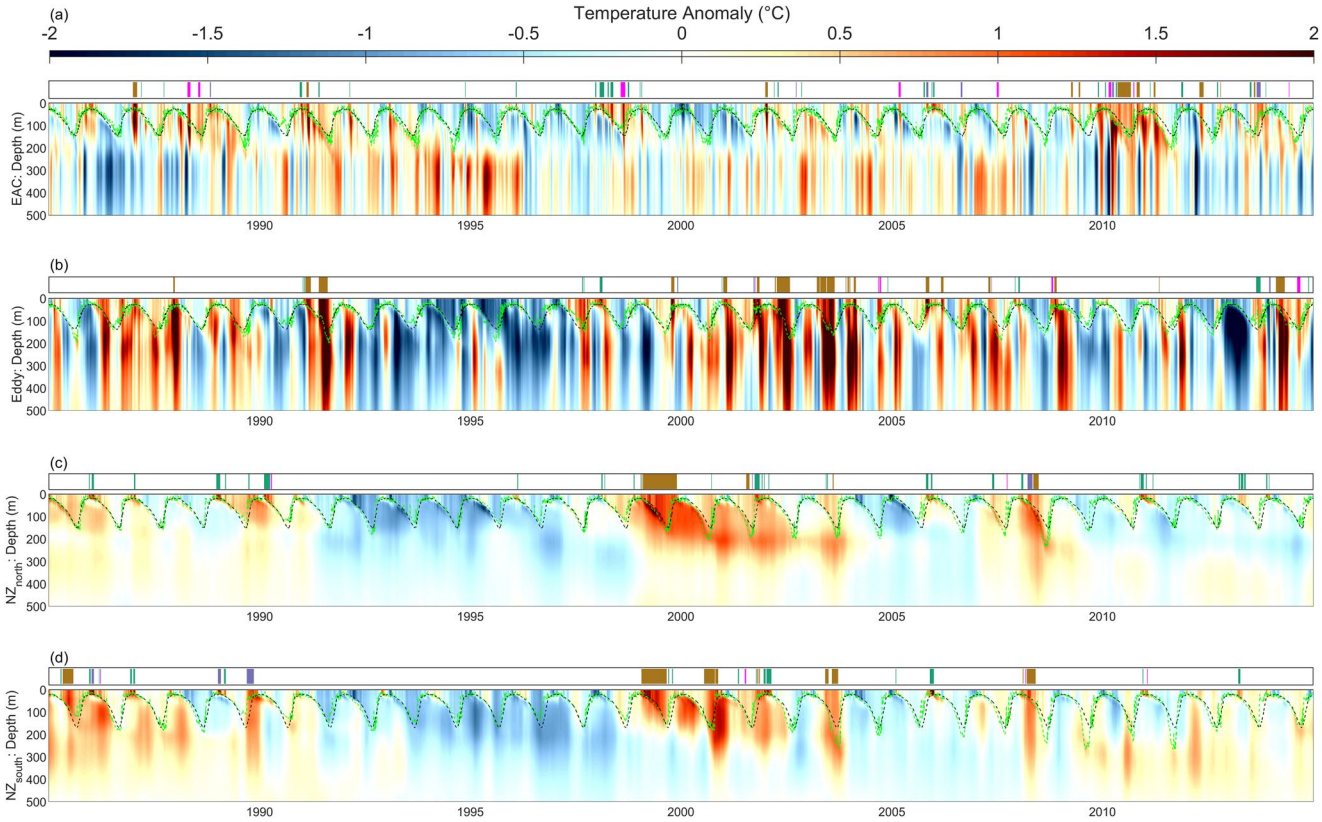

Figure 3. Hovmoller plots (depth vs. time) of the evolution of temperature anomalies from the surface to 500 m depth for each region for the period of 1985–2014. The dashed lines show the box's mixed layer depth (MLD, green) and climatological MLD (black). Marine heatwave occurrences are shown with colors corresponding to their dominant driver classification above each plot: Q' (green), Adv' (brown), Mixed (purple), and residual (magenta).

error (RMSE) (Figure S1). Correlations between Argo observations and OFAM3 (Figure S2), at depth, exceeded $r = 0.99$ (p-value $\ll 0.05$) with mean bias of -0.26°C, -0.15°C and 0.28°C in the EAC, Eddy and NZ_{south} boxes, respectively.

Over the period of 1985–2014, a total of 168 MHWs were identified, ~40 events in each box with the exception of EAC, which produced 53 events albeit of shorter durations (~16 days compared to ~20–30 days in the other regions). The evolution of temperature anomalies (Figure 3) for each box shows the individual MHWs identified in the surface MLD and illustrates the differences between the dynamical regions in terms of the temperature variability over depth. The variation in temperature anomalies on the west side of the Tasman Sea (EAC and Eddy boxes) are shorter, deeper and more barotropic than on the east side (NZ_{north} and NZ_{south}), where there is much less variability and many of the MHWs are mixed layer restricted, especially in the NZ_{north} box. The NZ_{south} box exhibits a mix of barotropic and mixed layer restricted temperature anomalies.

We found that the dominant drivers of heat variability were distinctively different over the east and west of the Tasman Sea but consistent along each coast (Figure S3). Off the east coast of Australia, in the EAC and Eddy boxes, advection was the dominant contributor of warming whilst air-sea heatflux cooled the areas on average. Off the west coast of New Zealand, the rate of change of temperature in the north and south boxes was mostly governed by air-sea heatflux with highly significant correlations of $r = 0.9$ (between the temperature tendency and air-sea heatflux, p-value $\ll 0.05$) across both boxes.

3.2. Drivers and Characteristics

While, generally, advection in the EAC was the warming contributor in the mixed layer temperature tendency, we found that MHWs were mostly driven by air-sea heatflux with 53% being Q'-MHWs and advection driving only 21% of events (Figure 4a). Conversely, in the EAC southern extension (Eddy box), Adv'-MHWs

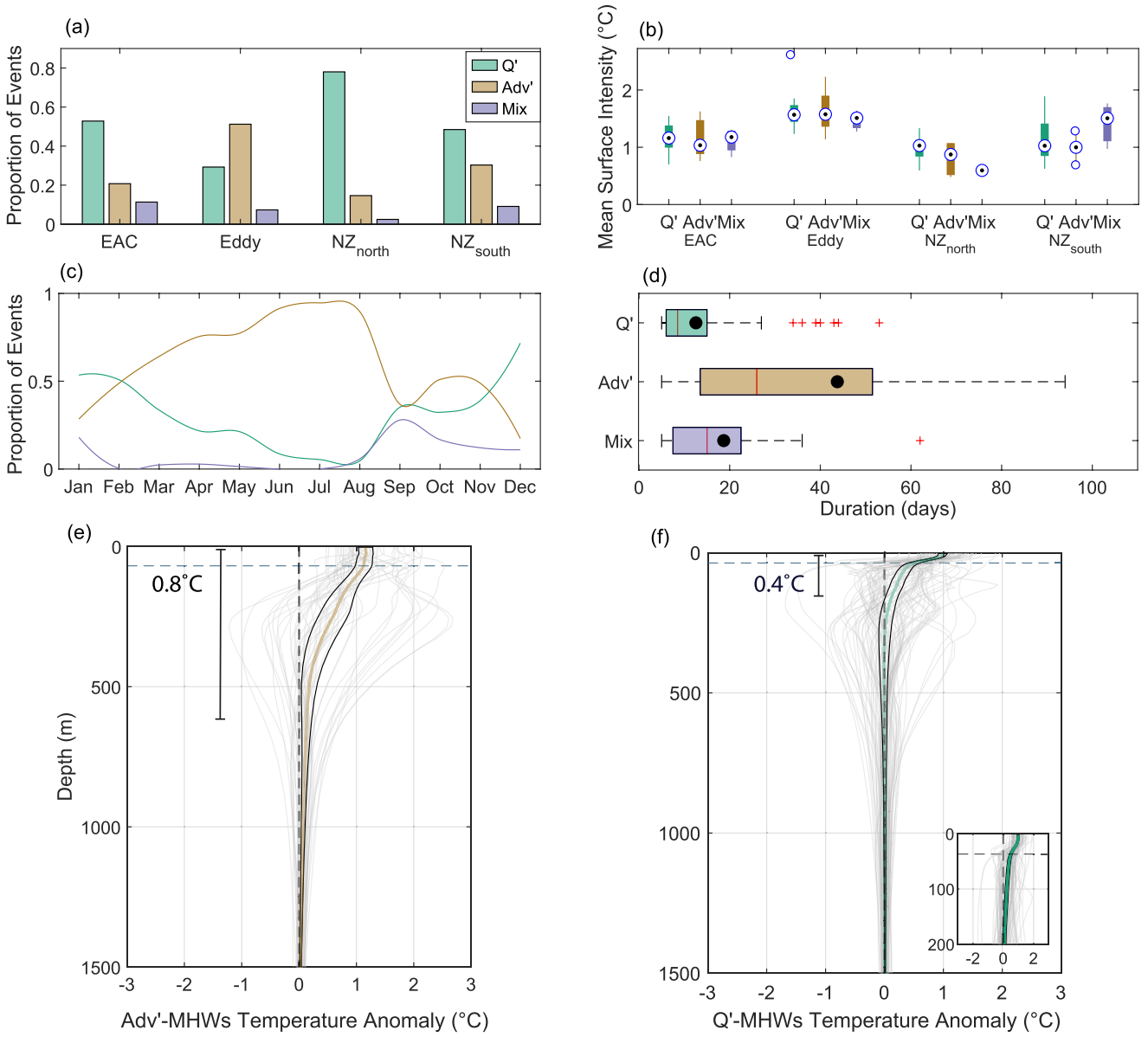

Figure 4. (a) Marine heatwave (MHW) frequency by dominant driver per box. Air-sea heatflux shown in green, advection in brown and mixed in purple. (b) Box plots showing MHW mean surface intensity by dominant driver per box. Panels (c–f) include all regions. (c) MHW days by dominant driver per month. (d) Box plots showing the spread of duration lengths of MHWs by dominant driver with median (red line) and mean (black solid circle). (e and f) Vertical profiles of temperature anomalies during MHWs driven by (e) advection and (f) air-sea heatflux. Thick lines show the mean profile (green and brown corresponding to driver), black solid lines indicate the 95% confidence interval and light gray lines show single profiles. MHW depth and vertical intensity, for the mean profile, are marked by the line segments and printed temperature anomalies. Mean MHW mixed layer depth is shown with the thin black dashed line.

and Q'-MHWs occurred at 51% and 29%, respectively. Over the four boxes, Adv'-MHWs only dominated in the Eddy box. Off the west coast of New Zealand, 80% of MHWs off the North Island were Q'-MHWs while, off the South Island 50% and 30% were Q'-MHWs and Adv'-MHWs, respectively. Mixed events were most frequent in the EAC and NZ_{south} regions, at 11% and 9% of MHWs respectively. Events classified as residual-driven comprised ~12% of all boxes except NZ_{north} where they constituted 5% of all events.

To investigate the drivers of the air-sea heatflux anomaly, we further explored individual flux components (sensible, latent, shortwave and longwave flux, Figure S4). Our results showed that latent flux anomaly was consistently the leading contributor to the warm air-sea heatflux anomaly across all boxes. In the Eddy region, however, shortwave flux was a comparably significant contributor to the warm anomaly with an

average contribution of $\sim 6 \times 10^{-3}$ °C/day and $\sim 8 \times 10^{-3}$ °C/day for shortwave and latent flux, respectively. The most intense air-sea heatflux anomalies occurred off the North Island of New Zealand.

MHW mean surface intensities (based on ML average, Figure 4b) showed that the most intense regions are Eddy and NZ_{south}, consistent with the 90^{th} percentile temperature anomaly spatial map (Figure 1b). It is also worth noting that there is almost no distinguishable surface temperature signal between drivers within regions.

When aggregating MHWs by their dominant drivers and out of their geographic context (Figure 4, panels c–f), we found 19 out of 168 events were residual-driven. A total of 88 MHWs were Q'-MHWs, 48 Adv'-MHWs and 13 mixed-driven. Adv'-MHWs had an average duration of 44 days, approximately four times longer than the 12 days of those driven by Q' (Figure 4d). Mixed-driven events (near equal contributions of Adv' and Q') lasted, on average, 19 days. Seasonality is shown in Figure 4c and is based on the proportion of MHW days per month by driver. A strong seasonal cycle exists in Q'-MHWs as expected, with most occurring in the austral summer (December–February) when the MLD is shallowest. Adv'-MHWs can occur year-round with a dephased seasonal cycle and mostly occur in autumn and winter (March–August). MHWs driven by a mix of both Adv' and Q' are most prevalent in spring, in particular during September.

3.3. MHW Depth

Departing from the mixed layer volume bounded analysis, we looked at the depth extent of the temperature anomalies during MHWs based on their dominant driver as determined above (Figures 4e, 4f, and S5). On average, anomalous warming is three times deeper in Adv'-MHWs than in those driven by surface forcing. Here, having applied the MHW depth definition to all the profiles (Figure S5) we found a depth median of 580 m with depth-averaged intensity (temperature anomaly from surface down to its corresponding MHW depth) of 0.9°C for Adv'-MHWs. Q'-MHWs produced a median MHW depth of 155 m with depth-averaged intensity of 0.3°C. This is illustrated in the average profiles (Figures 4e and 4f), where Adv'-MHW depth is at 685 m with depth-averaged intensity of ~0.8°C and Q'-MHW depth at 205 m and with half the intensity at ~0.4°C. In Adv'-MHWs, some profiles reached their maximum anomalies well below the mixed layer depth, occurring as deep as 250 m below the surface. Although, Adv'-MHWs are not necessarily describing eddy structures, those instances agree with results from Elzahaby and Schaeffer (2019), which showed that the deepest MHWs were associated with ocean advection through anticyclonic eddy structures in a region similar to the Eddy box. While the link between deep MHWs and eddies could be explained by isopycnal heave (Scannell et al., 2020), preliminary analysis showed no clear pattern between Adv'-MHWs and heave. In fact, spice could be an important factor in the region. More analysis is required to investigate the influence of isopycnal heave and water-mass variability on the sub-surface persistence and maximum MHW signals as identified by Scannell et al. (2020) in the evolution of the 2008/09 Northeast Pacific MHW.

The thermocline depth in the mean vertical profile of Q -MHWs was approximately 20–30 m with a temperature gradient of ~0.02°C/m. By contrast, the thermocline in the mean Adv' profile occurred between ~60 m and ~500 m with a temperature gradient of ~0.003°C/m. That is, in Q'-MHWs, the temperature anomalies decrease at a much higher rate in the surface layers, while the anomalies in Adv'-MHWs persist much deeper. We also found a significant correlation between dominant driver intensity and MHW depth with $r = -0.4$ and $r = 0.4$ for Q' and Adv', respectively. This means that the more intense the air-sea heatflux anomaly, the shallower the MHW. The inverse is true for Adv'-MHWs.

An analysis of the change in MLD during MHWs (Figure S6) shows that, on average, the MLD is 30% shallower during Q'-MHWs compared to its climatological depth across all boxes. In comparison negligible changes were found during Adv'-MHWs. Despite the large differences at depths, temperature anomalies for Adv'-MHWs and Q'-MHWs are similar near the surface, with an average of 1.1°C and 1°C, respectively (Figures 4e and 4f).

4. Discussion and Conclusions

Through our three-dimensional study of MHWs and their characteristics, discernible links are drawn between dominant drivers and characteristics in contrasting regions of the Tasman Sea. Adv'-MHWs result in more intense (at depth) and persistent events that penetrate well below the mixed layer. These MHWs average about 685 m in depth and last an average 45 days, with depth-averaged intensity of ∼0.8°C. They are more prevalent in autumn and winter. The depth of the MHW is positively correlated to the anomalous advection intensity during the event. In contrast, Q'-MHWs are more transient, generally restricted to the shallow surface mixed layer and have a strong seasonal cycle. The depth extent of the anomalous temperature reaches 205 m on average with ∼0.4°C mean intensity and last approximately 12 days. They mostly occur in the summer when the MLD is the shallowest. The depth penetration of the warm anomaly is negatively correlated to the Q' intensity, that is, the stronger the anomaly, the shallower the MHW. The temperature declines rapidly at depth, with a thermocline around 15 and 30 m. Interestingly, the difference between the surface temperature anomalies in both types of MHWs (Q' and Adv') is indistinguishable, further reinforcing the need to explore MHWs beyond SST.

Consistent with literature, we found that latent heatflux was the predominant anomaly in Q', that is, suppressed heat loss from anomalously weakened winds (Gupta et al., 2020; Salinger et al., 2020; Schlegel et al., 2021). Under these conditions, vertical mixing is reduced (less mixing with cooler waters beneath), which intensifies further surface warming as Salinger et al. (2020) outlined in the evolution of the 2017/18 MHW around New Zealand. The dominance of the latent flux anomaly, combined with the negative correlation between MHW depth and Q' intensity, infers that shoaling of the MLD may be enhancing or driving these events. On average, we found that MLD is ∼30% shallower during Q'-MHWs and unchanged during Adv'-MHWs. Further analysis would be beneficial to distinguish between the driving mechanisms in the lead-up to an event and during their onset (Schlegel et al., 2021). Also, further analysis should be conducted to confirm the dominance of latent flux in Q'-MHWs given the model's use of air-sea heatflux in avoiding temperature drifts (Oke et al., 2013). However, our results produced pronounced patterns and are consistent with findings of others.

Our findings suggest that the most intense and deepest MHWs, which pose the most ecological impact, are potentially easier to detect considering their longer durations. Consistent with our findings, Holbrook et al. (2020) showed that MHWs with strong oceanic contributions are deep (up to 100 s of meters). The longer durations of advection dominated MHWs, as shown through our study, implies that a dependence on daily sampling and thus the limitation of sub-surface observations becomes less critical for detecting this type of MHW. This knowledge combined with the findings laid out by the authors in Schlegel et al. (2019) on sub-optimal observations in MHW detection advances the possibility of monitoring sub-surface MHWs.

In the heat budget formulation, we used a time-varying mixed layer depth where effects of vertical mixing tend to diminish (compared to fixed layer budgets that may cut across the mixed layer) (Foltz et al., 2013; Ray et al., 2018) and therefore reduce the impact of having not resolved vertical terms in our equation. This method resulted in smaller residual variance than a fixed MLD in all four boxes with standard deviation of ∼0.02–0.03°C/day on average (other terms average 0.05–0.06°C/day). Overall, the statistical spread of the residual term (in all four regions) is small relative to Q and Adv (Figures S1b–S1h), giving confidence that the sum of Q and Adv describes most of the variability in temperature. Moreover, using the varying MLD captures events that are influenced by its variability like the New Zealand 2017/18 MHW, mentioned above, where shoaling of the ML can amplify air-sea heatflux impact. Even though we found residuals to be of insignificant consequence in our heat budget (the residual standard deviation was less than half the magnitude of other terms), the entrainment/detrainment term (included in our residual) could be influential in the lead up to MHWs and used to identify events where re-emergence processes are important. This is left for future work.

It is reasonable to posit that similar dynamical roles may be observed in other WBCs and atmospherically governed regions. We anticipate the WBC upstream to consist of more frequent and brief MHWs that are predominantly driven by air-sea heatflux and occur mostly around summer when the MLD is shallow, amplifying surface warming. We expect advection-dominated eddy (extension) regions to have the deepest and most vertically intense MHWs driven by anomalous advection. We also expect MHWs in air-sea

flux-controlled regions to be mostly restricted to the mixed layer, with more potential for events resulting from re-emergence of detrained waters. Continued sub-surface analysis surrounding MHWs is recommended to further progress the predictability of these catastrophic events.

Data Availability Statement

Publicly available data sets were analysed in this study. The OFAM3 model results are produced by CSIRO Ocean Downscaling Strategic Project in close collaboration with the Bluelink team (http://wp.csiro.au/bluelink/global/, https://geonetwork.nci.org.au/geonetwork/srv/eng/catalog.search#/metadata/f9007_2850_9392_7175). The Argo data were downloaded from the Australian Ocean Data Network portal (https://portal.aodn.org.au/, http://www.argodatamgt.org/Access-to-data) and these data were collected and made freely available by the International Argo Program and the national programs that contribute to it (https://argo.ucsd.edu, https://www.ocean-ops.org). NOAA_OI_SST_V2.1 data provided by the NOAA/OAR/ESRL PSD, Boulder, Colorado, United States, from their website at https://www.esrl.noaa.gov/psd/ (https://www.ncei.noaa.gov/thredds/blended-global/oisst-catalog.html).

Acknowledgments
This research was undertaken with the assistance of resources and services from the National Computational Infrastructure (NCI), which is supported by the Australian Government. The Argo Program is part of the Global Ocean Observing System (Argo, 2020). Argo data was sourced from Australia's Integrated Marine Observing System (IMOS)—IMOS is enabled by the National Collaborative Research Infrastructure Strategy (NCRIS). It is operated by a consortium of institutions as an unincorporated joint venture, with the University of Tasmania as Lead Agent. This work is a contribution to the Moana Project (www.moanaproject.org) funded by the New Zealand Ministry of Business Innovation and Employment, contract number MetO1801. This research was supported by an Australian Government Research Training Program (RTP) Scholarship.

References

Argo. (2020). Argo float data and metadata from Global Data Assembly Centre (Argo GDAC). *SEANOE*. https://doi.org/10.17882/42182

Banzon, V., Smith, T. M., Chin, T. M., Liu, C., & Hankins, W. (2016). A long-term record of blended satellite and in situ sea-surface temperature for climate monitoring, modeling and environmental studies. *Earth System Science Data*, *8*(1), 165–176. https://doi.org/10.5194/essd-8-165-2016

Banzon, V., Smith, T. M., Steele, M., Huang, B., & Zhang, H.-M. (2020). Improved estimation of proxy sea surface temperature in the arctic. *Journal of Atmospheric and Oceanic Technology*, *37*(2), 341–349. https://doi.org/10.1175/jtech-d-19-0177.1

Behrens, E., Hogg, A. M., England, M. H., & Bostock, H. (2020). *Seasonal and interannual variability of the subtropical front in the New Zealand region*. https://doi.org/10.1002/essoar.10503132.1

Benthuysen, J., Feng, M., & Zhong, L. (2014). Spatial patterns of warming off Western Australia during the 2011 Ningaloo Niño: Quantifying impacts of remote and local forcing. *Continental Shelf Research*, *91*, 232–246. https://doi.org/10.1016/j.csr.2014.09.014

Benthuysen, J., Oliver, E., Feng, M., & Marshall, A. G. (2018). Extreme marine warming across tropical Australia during austral summer 2015–2016. *Journal of Geophysical Research: Oceans*, *123*(2), 1301–1326. https://doi.org/10.1002/2017jc013326

Bowen, M., Markham, J., Sutton, P., Zhang, X., Wu, Q., Shears, N. T., & Fernandez, D. (2017). Interannual variability of sea surface temperature in the southwest pacific and the role of ocean dynamics. *Journal of Climate*, *30*(18), 7481–7492. https://doi.org/10.1175/jcli-d-16-0852.1

Chen, K., Gawarkiewicz, G. G., Lentz, S. J., & Bane, J. M. (2014). Diagnosing the warming of the northeastern U.S. coastal ocean in 2012: A linkage between the atmospheric jet stream variability and ocean response. *Journal of Geophysical Research: Oceans*, *119*(1), 218–227. https://doi.org/10.1002/2013jc009393

Chen, K., Gawarkiewicz, G., Kwon, Y.-O., & Zhang, W. G. (2015). The role of atmospheric forcing versus ocean advection during the extreme warming of the northeast U.S. continental shelf in 2012. *Journal of Geophysical Research: Oceans*, *120*(6), 4324–4339. https://doi.org/10.1002/2014jc010547

de Boyer Montégut, C. (2004). Mixed layer depth over the global ocean: An examination of profile data and a profile-based climatology. *Journal of Geophysical Research*, *109*(C12), C12003. https://doi.org/10.1029/2004jc002378

Dee, D. P., & Uppala, S. (2009). Variational bias correction of satellite radiance data in the ERA-interim reanalysis. *Quarterly Journal of the Royal Meteorological Society*, *135*(644), 1830–1841. https://doi.org/10.1002/qj.493

Elzahaby, Y., & Schaeffer, A. (2019). Observational insight into the subsurface anomalies of marine heatwaves. *Frontiers in Marine Science*, *6*. https://doi.org/10.3389/fmars.2019.00745

Feng, M., McPhaden, M. J., Xie, S.-P., & Hafner, J. (2013). La niña forces unprecedented leeuwin current warming in 2011. *Scientific Reports*, *3*(1), 1277. https://doi.org/10.1038/srep01277

Feng, M., Zhang, X., Oke, P., Monselesan, D., Chamberlain, M., Matear, R., & Schiller, A. (2016). Invigorating ocean boundary current systems around Australia during 1979–2014: As simulated in a near-global eddy-resolving ocean model. *Journal of Geophysical Research: Oceans*, *121*(5), 3395–3408. https://doi.org/10.1002/2016jc011842

Foltz, G. R., Schmid, C., & Lumpkin, R. (2013). Seasonal cycle of the mixed layer heat budget in the northeastern tropical Atlantic ocean. *Journal of Climate*, *26*(20), 8169–8188. https://doi.org/10.1175/jcli-d-13-00037.1

Frölicher, T. L., Fischer, E. M., & Gruber, N. (2018). Marine heatwaves under global warming. *Nature*, *560*(7718), 360–364. https://doi.org/10.1038/s41586-018-0383-9

Gawarkiewicz, G., Chen, K., Forsyth, J., Bahr, F., Mercer, A. M., Ellertson, A., et al. (2019). Characteristics of an advective marine heatwave in the middle Atlantic bight in early 2017. *Frontiers in Marine Science*, *6*. https://doi.org/10.3389/fmars.2019.00712

Griffies, S. M., Schmidt, M., & Herzfeld, M. (2009). Elements of mom4p1. In *GFDL Ocean Group Technical Report 6*. (p. 444).

Gupta, A. S., Thomsen, M., Benthuysen, J. A., Hobday, A. J., Oliver, E., Alexander, L. V., et al. (2020). Drivers and impacts of the most extreme marine heatwaves events. *Scientific Reports*, *10*(1). https://doi.org/10.1038/s41598-020-75445-3

Hayashida, H., Matear, R. J., Strutton, P. G., & Zhang, X. (2020). Insights into projected changes in marine heatwaves from a high-resolution ocean circulation model. *Nature Communications*, *11*(1). https://doi.org/10.1038/s41467-020-18241-x

Heath, R. (1981). Oceanic fronts around southern New Zealand. Deep Sea Research Part A. *Oceanographic Research Papers*, *28*(6), 547–560. https://doi.org/10.1016/0198-0149(81)90116-3

Hill, K. L., Rintoul, S. R., Ridgway, K. R., & Oke, P. R. (2011). Decadal changes in the south pacific western boundary current system revealed in observations and ocean state estimates. *Journal of Geophysical Research*, *116*(C1). https://doi.org/10.1029/2009jc005926

Hobday, A., Alexander, L., Perkins, S. E., Smale, D. A., Straub, S. C., Oliver, E. C., et al. (2016). A hierarchical approach to defining marine heatwaves. *Progress in Oceanography*, *141*, 227–238. https://doi.org/10.1016/j.pocean.2015.12.014

Hobday, A., Oliver, E., Gupta, A. S., Benthuysen, J., Burrows, M., Donat, M., et al. (2018). Categorizing and naming marine heatwaves. *Oceanography*, *31*(2). https://doi.org/10.5670/oceanog.2018.205

Holbrook, N. J., Gupta, A. S., Oliver, E. C. J., Hobday, A. J., Benthuysen, J. A., Scannell, H. A., et al. (2020). Keeping pace with marine heatwaves. *Nature Reviews Earth & Environment*, *1*(9), 482–493. https://doi.org/10.1038/s43017-020-0068-4

Huang, B., Liu, C., Banzon, V., Freeman, E., Graham, G., Hankins, B., et al. (2021). Improvements of the daily optimum interpolation sea surface temperature (DOISST) version 2.1. *Journal of Climate*, *34*(8), 2923–2939. https://doi.org/10.1175/jcli-d-20-0166.1

Jackson, J. M., Johnson, G. C., Dosser, H. V., & Ross, T. (2018). Warming from recent marine heatwave lingers in deep British Columbia fjord. *Geophysical Research Letters*, *45*(18), 9757–9764. https://doi.org/10.1029/2018gl078971

Li, Z., Holbrook, N. J., Zhang, X., Oliver, E. C. J., & Cougnon, E. A. (2020). Remote forcing of Tasman Sea marine heatwaves. *Journal of Climate*, *33*(12), 5337–5354. https://doi.org/10.1175/jcli-d-19-0641.1

Marzinelli, E. M., Williams, S. B., Babcock, R. C., Barrett, N. S., Johnson, C. R., Jordan, A., et al. (2015). Large-scale geographic variation in distribution and abundance of Australian deep-water kelp forests. *PloS One*, *10*(2), e0118390. https://doi.org/10.1371/journal.pone.0118390

Nilsson, C., & Cresswell, G. (1980). The formation and evolution of East Australian Current warm-core eddies. *Progress in Oceanography*, *9*(3), 133–183. https://doi.org/10.1016/0079-6611(80)90008-7

Oke, P. R., Griffin, D. A., Schiller, A., Matear, R. J., Fiedler, R., Mansbridge, J., et al. (2013). Evaluation of a near-global eddy-resolving ocean model. *Geoscientific Model Development*, *6*(3), 591–615. https://doi.org/10.5194/gmd-6-591-2013

Oke, P. R., Roughan, M., Cetina-Heredia, P., Pilo, G. S., Ridgway, K. R., Rykova, T., et al. (2019). Revisiting the circulation of the East Australian Current: Its path, separation, and eddy field. *Progress in Oceanography*, *176*, 102139. https://doi.org/10.1016/j.pocean.2019.102139

Oliver, E. C. J., Benthuysen, J. A., Bindoff, N. L., Hobday, A. J., Holbrook, N. J., Mundy, C. N., & Perkins-Kirkpatrick, S. E. (2017). The unprecedented 2015/16 Tasman Sea marine heatwave. *Nature Communications*, *8*(1). https://doi.org/10.1038/ncomms16101

Oliver, E. C. J., Burrows, M. T., Donat, M. G., Gupta, A. S., Alexander, L. V., Perkins-Kirkpatrick, S. E., et al. (2019). Projected marine heatwaves in the 21st century and the potential for ecological impact. *Frontiers in Marine Science*, *6*. https://doi.org/10.3389/fmars.2019.00734

Pilo, G. S., Holbrook, N. J., Kiss, A. E., & Hogg, A. M. (2019). Sensitivity of marine heatwave metrics to ocean model resolution. *Geophysical Research Letters*, *46*(24), 14604–14612. https://doi.org/10.1029/2019gl084928

Popova, E., Yool, A., Byfield, V., Cochrane, K., Coward, A. C., Salim, S. S., et al. (2016). From global to regional and back again: Common climate stressors of marine ecosystems relevant for adaptation across five ocean warming hotspots. *Global Change Biology*, *22*(6), 2038–2053. https://doi.org/10.1111/gcb.13247

Ray, S., Wittenberg, A. T., Griffies, S. M., & Zeng, F. (2018). Understanding the equatorial pacific cold tongue time-mean heat budget. Part I: Diagnostic framework. *Journal of Climate*, *31*(24), 9965–9985. https://doi.org/10.1175/jcli-d-18-0152.1

Reynolds, R. W., Smith, T. M., Liu, C., Chelton, D. B., Casey, K. S., & Schlax, M. G. (2007). Daily high-resolution-blended analyses for sea surface temperature. *Journal of Climate*, *20*(22), 5473–5496. https://doi.org/10.1175/2007jcli1824.1

Rodrigues, R. R., Taschetto, A. S., Gupta, A. S., & Foltz, G. R. (2019). Common cause for severe droughts in South America and marine heatwaves in the South Atlantic. *Nature Geoscience*, *12*(8), 620–626. https://doi.org/10.1038/s41561-019-0393-8

Roemmich, D., Johnson, G., Riser, S., Davis, R., Gilson, J., Owens, W. B., et al. (2009). The argo program: Observing the global oceans with profiling floats. *Oceanography*, *22*(2), 34–43. https://doi.org/10.5670/oceanog.2009.36

Rykova, T., & Oke, P. R. (2015). Recent freshening of the East Australian Current and its eddies. *Geophysical Research Letters*, *42*(21), 9369–9378. https://doi.org/10.1002/2015gl066050

Salinger, M. J., Diamond, H. J., Behrens, E., Fernandez, D., Fitzharris, B. B., Herold, N., et al. (2020). Unparalleled coupled ocean-atmosphere summer heatwaves in the New Zealand region: Drivers, mechanisms and impacts. *Climatic Change*, *162*, 485–506. https://doi.org/10.1007/s10584-020-02730-5

Salinger, M. J., Renwick, J., Behrens, E., Mullan, A. B., Diamond, H. J., Sirguey, P., et al. (2019). The unprecedented coupled ocean-atmosphere summer heatwave in the new zealand region 2017/18: Drivers, mechanisms and impacts. *Environmental Research Letters*, *14*(4), 044023. https://doi.org/10.1088/1748-9326/ab012a

Scannell, H. A., Johnson, G. C., Thompson, L., Lyman, J. M., & Riser, S. C. (2020). Subsurface evolution and persistence of marine heatwaves in the northeast pacific. *Geophysical Research Letters*, *47*(23). https://doi.org/10.1029/2020gl090548

Schaeffer, A., & Roughan, M. (2017). Subsurface intensification of marine heatwaves off southeastern Australia: The role of stratification and local winds. *Geophysical Research Letters*, *44*(10), 5025–5033. https://doi.org/10.1002/2017gl073714

Schlegel, R. W., Oliver, E. C. J., & Chen, K. (2021). Drivers of marine heatwaves in the northwest Atlantic: The role of air–sea interaction during onset and decline. *Frontiers in Marine Science*, *8*. https://doi.org/10.3389/fmars.2021.627970

Schlegel, R. W., Oliver, E. C. J., Hobday, A. J., & Smit, A. J. (2019). Detecting marine heatwaves with sub-optimal data. *Frontiers in Marine Science*, *6*. https://doi.org/10.3389/fmars.2019.00737

Schlundt, M., Brandt, P., Dengler, M., Hummels, R., Fischer, T., Bumke, K., et al. (2014). Mixed layer heat and salinity budgets during the onset of the 2011 Atlantic cold tongue. *Journal of Geophysical Research: Oceans*, *119*(11), 7882–7910. https://doi.org/10.1002/2014jc010021

Short, J., Foster, T., Falter, J., Kendrick, G. A., & McCulloch, M. T. (2015). Crustose coralline algal growth, calcification and mortality following a marine heatwave in Western Australia. *Continental Shelf Research*, *106*, 38–44. https://doi.org/10.1016/j.csr.2015.07.003

Smale, D. A., Wernberg, T., Oliver, E. C. J., Thomsen, M., Harvey, B. P., Straub, S. C., et al. (2019). Marine heatwaves threaten global biodiversity and the provision of ecosystem services. *Nature Climate Change*, *9*(4), 306–312. https://doi.org/10.1038/s41558-019-0412-1

Smith, R. O., Vennell, R., Bostock, H. C., & Williams, M. J. (2013). Interaction of the subtropical front with topography around southern New Zealand. *Deep Sea Research Part I: Oceanographic Research Papers*, *76*, 13–26. https://doi.org/10.1016/j.dsr.2013.02.007

Stammer, D., Balmaseda, M., Heimbach, P., Köhl, A., & Weaver, A. (2016). Ocean data assimilation in support of climate applications: Status and perspectives. *Annual Review of Marine Science*, *8*(1), 491–518. https://doi.org/10.1146/annurev-marine-122414-034113

Stevenson, J. W., & Niiler, P. P. (1983). Upper ocean heat budget during the hawaii-to-tahiti shuttle experiment. *Journal of Physical Oceanography*, *13*(10), 1894–1907. https://doi.org/10.1175/1520-0485(1983)013<1894:uohbdt>2.0.co;2

Sutton, P. J. H., & Bowen, M. (2019). Ocean temperature change around New Zealand over the last 36 years. *New Zealand Journal of Marine & Freshwater Research*, *53*(3), 305–326. https://doi.org/10.1080/00288330.2018.1562945

Tranter, D. J., Parker, R. R., & Cresswell, G. R. (1980). Are warm-core eddies unproductive? *Nature*, *284*(5756), 540–542. https://doi.org/10.1038/284540a0

Wang, W., & McPhaden, M. J. (1999). The surface-layer heat balance in the equatorial Pacific Ocean. Part I: Mean seasonal cycle. *Journal of Physical Oceanography*, *29*(8), 1812–1831. https://doi.org/10.1175/1520-0485(1999)029<1812:tslhbi>2.0.co;2

Wernberg, T. (2020). Marine heatwave drives collapse of kelp forests in Western Australia. In Canadell, J. G., & In Jackson, R. B. (Eds.), *Ecosystem collapse and climate change. Ecological studies*. Springer-Nature.

Wernberg, T., Smale, D., Tuya, F., Thomsen, M., Langlois, T., De Bettignies, T., & Rousseaux, C. (2013). An extreme climatic event alters marine ecosystem structure in a global biodiversity hotspot. *Nature Climate Change*, *3*. https://doi.org/10.1038/NCLIMATE1627

Wu, L., Cai, W., Zhang, L., Nakamura, H., Timmermann, A., Joyce, T., et al. (2012). Enhanced warming over the global subtropical western boundary currents. *Nature Climate Change*, *2*(3), 161–166. https://doi.org/10.1038/nclimate1353